Monthly Notices
of the
ROYAL ASTRONOMICAL SOCIETY

MNRAS **429,** 2469–2481 (2013) doi:10.1093/mnras/sts516

Fluctuation dynamos and their Faraday rotation signatures

Pallavi Bhat⋆ and Kandaswamy Subramanian

IUCAA, Post Bag 4, Ganeshkhind, Pune 411007, India

Accepted 2012 November 28. Received 2012 November 28; in original form 2012 October 10

ABSTRACT

Turbulence is ubiquitous in many astrophysical systems like galaxies, galaxy clusters and possibly even the filaments in the intergalactic medium. We study fluctuation dynamo action in turbulent systems focusing on one observational signature, the random Faraday rotation measure (RM) from radio emission of background sources seen through the intermittent magnetic field generated by such a dynamo. We simulate the fluctuation dynamo in periodic boxes up to resolutions of 512^3, with varying fluid and magnetic Reynolds numbers, and measure the resulting random RMs. We show that even though the magnetic field generated is intermittent, it still allows for contributions to the RM to be significant. When the dynamo saturates, the rms value of RM is of the order of 40–50 per cent of the value expected in a model where fields of strength $B_{\rm rms}$ uniformly fill cells of the largest turbulent eddy but are randomly oriented from one cell to another. This level of RM dispersion is obtained across different values of magnetic Reynolds number and Prandtl number explored. We also use the random RMs to probe the structure of the generated fields to distinguish the contribution from intense and diffuse field regions. We find that the strong field regions (say with $B > 2B_{\rm rms}$) contribute only of the order of 15–20 per cent to the RM. Thus, rare structures do not dominate the RM; rather, the general 'sea' of volume filling fluctuating fields are the dominant contributors. We also show that the magnetic integral scale, $L_{\rm int}$, which is directly related to the RM dispersion, increases in all the runs, as Lorentz forces become important to saturate the dynamo. It appears that due to the ordering effect of the Lorentz forces, $L_{\rm int}$ of the saturated field tends to a modest fraction, 1/2–1/3 of the integral scale of the velocity field, for all our runs. These results are then applied to discuss the Faraday rotation signatures of fluctuation dynamo generated fields in young galaxies, galaxy clusters and intergalactic filaments.

Key words: dynamo – MHD – turbulence – galaxies: clusters: general – galaxies: magnetic fields.

1 INTRODUCTION

The plasma in disc galaxies and that in galaxy clusters are observed to be magnetized. Disc galaxies have a large-scale component of the magnetic field ordered on kpc scales with a strength of several microgauss (μG) and a somewhat larger random component with coherence scales of tens of parsecs (Fletcher 2011; Beck 2012). Statistical studies of Faraday rotation in several galaxy clusters suggest that the intracluster medium also hosts a random field, with coherence scales of several kpc to tens of kpc and a strength of several μG, which goes up to tens of μG at the centre of cool core clusters (Clarke, Kronberg & Böhringer 2001; Govoni & Feretti 2004; Murgia et al. 2004; Vogt & Enßlin 2005; Bonafede et al. 2010; Govoni et al. 2010; Kuchar & Enßlin 2011). Moreover, there is evidence of ordered μG fields in high-redshift galaxies at $z \sim 1$, inferred from the statistical excess of Faraday rotation seen in distant quasars which have a Mg II absorption system in their spectra (Bernet et al. 2008). Understanding the origin of these ordered fields presents an important challenge.

Cosmic magnetic fields are thought to be generated by dynamo amplification of weak seed fields. Dynamos convert the kinetic energy of fluid motions to magnetic energy. Dynamos are particularly easy to excite in a sufficiently conducting plasma which hosts random or turbulent motions. In galaxies, turbulence can be driven by randomly occurring supernovae (SNe; Korpi et al. 1999; Balsara & Kim 2005; de Avillez & Breitschwerdt 2005; Gressel et al. 2008; Wu et al. 2009; Gent et al. 2012). In galaxy clusters and the general intergalactic medium, turbulence could arise from cluster mergers and structure formation shocks (Norman & Bryan 1999; Ryu et al. 2008; Xu et al. 2009; Iapichino et al. 2011; Paul et al. 2011; Vazza et al. 2011; Ryu et al. 2012). Such cosmological simulations show that the resulting turbulent velocities in the cluster plasma are highly subsonic and hence nearly incompressible. Evidence for cluster

⋆ E-mail: palvi@iucaa.ernet.in

turbulence to be nearly incompressible also comes from observations of pressure fluctuations (Schuecker et al. 2004; Churazov et al. 2012), and upper limits based on the width of X-ray emission lines (Sanders et al. 2010; Sanders, Fabian & Smith 2011; Sanders & Fabian 2012).

Such vortical turbulent motions generically lead to what is referred to as a fluctuation or small-scale dynamo under a modest condition that the magnetic Reynolds number $R_{\rm M}$ exceeds a critical value $R_{\rm crit}$ of the order of a few tens (Kazantsev 1968; Kulsrud & Anderson 1992; Subramanian 1999; Cho & Vishniac 2000; Haugen, Brandenburg & Dobler 2004a; Schekochihin et al. 2004; Brandenburg & Subramanian 2005; Cho et al. 2009; Tobias, Cattaneo & Boldyrev 2011; Brandenburg, Sokoloff & Subramanian 2012). The fluctuation dynamo amplifies magnetic fields on the fast eddy turnover time-scales (typically much smaller than the age of the system), on coherence scales smaller than the outer scale of the turbulence. On the other hand, mean-field or large-scale dynamos, which amplify fields correlated on scales larger than the turbulent eddy scales, typically require more special conditions (like turbulence to be helical) and operate on a much longer time-scale. Thus, the fluctuation dynamos will be important in all astrophysical systems, from young galaxies (where they probably generate the first fields) to galaxy clusters and intergalactic filaments (where conditions for mean-field dynamo action are likely to be absent).

The rapid amplification by fluctuation dynamos comes at a cost. The field is squeezed into smaller and smaller volumes, as rapidly as it is amplified, and gets highly intermittent in the kinematic stage (Zeldovich, Ruzmaikin & Sokoloff 1990). A critical issue for astrophysical applications is how coherent are the fields when the fluctuation dynamo saturates (Subramanian 1999; Haugen, Brandenburg & Dobler 2003; Haugen et al. 2004a; Schekochihin et al. 2004; Enßlin & Vogt 2006; Subramanian, Shukurov & Haugen 2006; Cho & Ryu 2009). Using simulations done with large magnetic Prandtl numbers ($P_{\rm M} = R_{\rm M}/Re > 1$), but small fluid Reynolds numbers (Re), Schekochihin et al. (2004) argued that the fluctuation dynamo generated fields saturate with a folded structure, where the fields reverse at the folds with the power concentrating on resistive scales $l_d \sim l/R_{\rm M}^{1/2}$ (l is the forcing scale of the turbulence). For large $R_{\rm M} \gg 1$ typical of astrophysical systems, this would lead to negligible Faraday rotation measure (RM). Simulations of Haugen et al. (2003, 2004a, hereafter HBD) with $P_{\rm M} = 1$ and a large $R_{\rm M} = Re = 960$ found that the magnetic correlation function $w(r) = \langle \boldsymbol{B}(\boldsymbol{x}) \cdot \boldsymbol{B}(\boldsymbol{x}+\boldsymbol{r})\rangle$ has a correlation scale $\sim 1/6$ of the scale of the corresponding velocity correlation function, but much larger than the resistive scale. This seems consistent with a simple model of Subramanian (1999, hereafter S99) for non-linear saturation of small-scale dynamos, which predicts that the power in the saturated state concentrates on scales $l_c \sim l/R_{\rm crit}^{1/2}$. One could then expect significant RMs, as is also consistent with the results of Subramanian et al. (2006, hereafter SSH) and Cho & Ryu (2009, hereafter CR09). The case when both Re and $P_{\rm M}$ are large, as in galactic and cluster plasmas, is not easy to simulate.[1] Indeed, the saturation of fluctuation dynamos could be quite different in large-Re turbulent systems which display what is called 'spontaneous stochasticity', compared to laminar high-$P_{\rm M}$ systems (Eyink 2011; Beresnyak 2012).

Note that Faraday rotation measurements are crucial to infer the presence of coherent magnetic fields. Therefore, it is especially important to understand how much Faraday rotation is produced if one sees a polarized radio source through the possibly intermittent magnetic field generated by a fluctuation dynamo. Addressing this question will form the focus of the present work. Some work on the RM from fluctuation dynamos has been done by SSH and CR09. We will consider here higher resolution simulations (up to 512^3) compared to SSH. We however follow SSH in computing the RM by directly integrating along a large number of lines of sight (LOS) (unlike CR09 who related the dispersion in RM to the energy spectrum assuming isotropy). We also extensively examine the sensitivity of the RM obtained from fluctuation dynamos to variation of both $R_{\rm M}$ and $P_{\rm M}$ (compared to both SSH and CR09). Moreover, unlike earlier woks, we will also resolve the contribution to the RM from high-field structures (where the field is much larger than the rms value) compared to the general volume filling field. This can also help probe the structure of the dynamo generated fields.

The next section presents the simulations that we have carried out to use for the RM analysis. Section 3 sets out the methodology for calculating the Faraday RM from the simulations and the results are presented in Section 4. Application of these results to astrophysical systems is considered in Section 5. The last section presents a discussion of these results and our conclusions.

2 SIMULATIONS OF FLUCTUATION DYNAMOS

In order to study the Faraday rotation signatures of fluctuation dynamos, we have run a suite of simulations using the PENCIL CODE (http://pencil-code.googlecode.com; Brandenburg & Dobler 2002; Brandenburg 2003). The PENCIL CODE uses a sixth-order finite difference in space and a third-order accurate time stepping method. The continuity, Navier–Stokes and induction equations are solved in a Cartesian box of size 2π on a cubic grid with N^3 mesh points, adopting periodic boundary conditions. The fluid is assumed to be isothermal, viscous, electrically conducting and mildly compressible. The code uses dimensionless quantities by measuring length in units of $L/2\pi$ (where L is the size of the box), speed in units of the isothermal sound speed $c_{\rm s}$, density in units of initial value ρ_0 and magnetic field in units of $(4\pi\rho_0 c_{\rm s}^2)^{1/2}$. To generate turbulent flow, a random force is included manifestly in the momentum equation. In Fourier space, this driving force is transverse to the wavevector $\boldsymbol{k}$ and localized in wavenumber space about a wavenumber $k_{\rm f}$. It drives vortical motions in a wavelength range around $2\pi/k_{\rm f}$, which will also be the energy carrying scales of the turbulent flow. The direction of the wavevector and its phase are changed at every time step in the simulation making the force almost δ-correlated in time (see HBD for details). For all our simulations, we choose to drive the motions between wavenumbers of 1 and 2, and thus the average $k_{\rm f} = 1.5$. This choice is motivated by the fact that we wish to resolve the small magnetic field scale structures in any turbulent cell as well as possible. The strength of the forcing is adjusted so that the rms Mach number of the turbulence, $u_{\rm rms}$ in the code (where velocity is measured in units of the isothermal sound speed), is typically about 0.15. This also implies that the motions are nearly incompressible. The magnetic and fluid Reynolds numbers throughout this paper are defined by $R_{\rm M} = u_{\rm rms}/\eta k_{\rm f}$ and $Re = u_{\rm rms}/\nu k_{\rm f}$, where η and ν are the resistivity and viscosity of the fluid. The magnetic Prandtl number is defined as $P_{\rm M} = R_{\rm M}/Re = \nu/\eta$.

[1] If one uses the *Spitzer* values for viscosity and resistivity, one gets $Re \sim 10^7$, $R_{\rm M} \sim 10^{18}$ in the galactic interstellar medium (ISM), while $Re \sim 1$ and $R_{\rm M} \sim 10^{29}$ for cluster plasma (Brandenburg & Subramanian 2005). However, in galaxy clusters, the viscosity (hence Re) and perhaps the resistivity (hence $R_{\rm M}$) are likely to be set by plasma effects (Schekochihin et al. 2005) rather than coulomb collisions, and then Re would increase and $R_{\rm M}$ would decrease, although their exact values are uncertain.

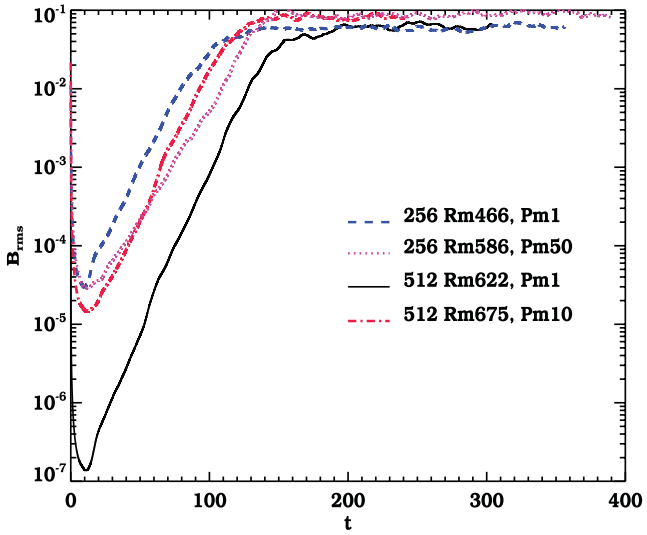

Figure 1. The evolution of $B_{\rm rms}$ with time for fluctuation dynamo simulations adopting $P_{\rm M} = 1$ and $P_{\rm M} > 1$ in both 256^3 and 512^3 resolutions. The black solid, blue dashed, red dash–dotted and pink dotted lines represent simulation runs F, B, G and D, respectively.

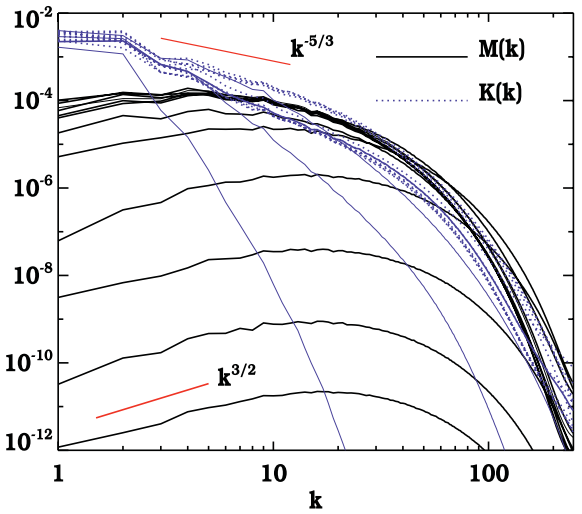

Figure 2. The time evolution of the kinetic $K(k)$ and magnetic $M(k)$ spectra for the 512^3 simulation of fluctuation dynamos with $R_{\rm M} = Re = 622$ (run F). The first time for the spectra is $43t_0$. The time difference between successive spectra is about $\sim 22t_0$.

Starting with a weak Gaussian random seed magnetic field, and for $R_{\rm M}$ above a critical value, the rms magnetic field $B_{\rm rms}$ first grows exponentially as shown in Fig. 1, before saturating (qualitatively similar to that by HBD and in the cosmological context; by Beck et al. 2012). The time in this and other figures is measured in units of the eddy turnover time $t_0 = (u_{\rm rms}k_{\rm f})^{-1}$, on the forcing scale $k_{\rm f}$. The simulation is allowed to run well into saturation as we want to calculate RM from the fields starting from the kinematic stage (when Lorentz forces are not important) up to the saturated stage. We have run simulations with a resolution up to 512^3 mesh points, with different $R_{\rm M}$ and $P_{\rm M}$ to be able to test the sensitivity of the resulting RM with respect to these parameters. These simulations adopt either $P_{\rm M} = 1$ or $P_{\rm M} > 1$ (note that we have also considered $P_{\rm M} > 1$ cases and not $P_{\rm M} < 1$, as the former case is more applicable to galactic and cluster plasmas). We give in Table 1, a summary of the parameters for all the runs. These include the number of mesh points N, η, ν, the resulting $u_{\rm rms}$ in the kinematic stage, the average $b_{\rm rms}$ at the saturated state, and $P_{\rm M}$ and $R_{\rm M}$ calculated using $u_{\rm rms}$.

The time evolution of the kinetic and magnetic spectra, $K(k, t)$ and $M(k, t)$, respectively, is shown in Fig. 2 for one of our higher resolution (512^3) simulations, with $R_{\rm M} = Re = 622$ (run F). The magnetic spectra are shown as black solid lines while the kinetic spectra as blue dotted lines, except for the final time, where it is shown as a thick solid line. (The buildup of the kinetic spectra is also shown as thin solid lines for three early times.) The two short red solid lines with power-law behaviour of the forms $k^{3/2}$ and $k^{-5/3}$ are shown for comparison with the Kazantsev and Kolmogorov spectra. We see that the kinetic spectra eventually develop an inertial range with a power-law behaviour slightly steeper than a Kolmogorov slope of $-5/3$. The magnetic spectra at early times have a Kazantsev form, $M(k) \propto k^{3/2}$ at small k, and are peaked at $k \sim 15$. However, as the field saturates the peak of $M(k)$ shifts to a much smaller $k \sim 4$, with $M(k)$ decreasing with k for larger k. These spectra are qualitatively similar to those obtained by HBD in their earlier work.

For $P_{\rm M} > 1$ runs, we have kept η the same as in the $P_{\rm M} = 1$ runs of the corresponding resolution and increased ν. The reason for not decreasing η instead is that the η for various $P_{\rm M} = 1$ runs are already set to almost their minimal values, if one takes care to resolve the smallest dissipative scales.[2] The time evolution of the corresponding kinetic and magnetic spectra, for a fluctuation dynamo simulation with $P_{\rm M} = 10$ and $R_{\rm M} = 675$ (run F), is shown in Fig. 3. The kinetic spectra cut off much more sharply than $k^{-5/3}$, as the fluid is now much more viscous. The magnetic spectra are also flatter at early times than the Kazantsev form, although still peaked at a large $k \sim 9$. As the field saturates, the peak of $M(k)$ shifts again to a much smaller $k \sim 5$, with $M(k)$ subsequently decreasing with k. These spectra are also qualitatively similar to the high-$P_{\rm M}$, high-Re spectra presented in Brandenburg & Subramanian (2005). We shall say more about these spectra later below. We now turn to an analysis of these simulations to find the RM predicted by the fluctuation dynamo.

Table 1. The parameters for various simulation runs in dimensionless units. Here $k_{\rm f} = 1.5$ for all the runs. The $u_{\rm rms}$ is that which is obtained in the kinematic stage while $b_{\rm rms}$ is the average value in the saturated state.

Run	Resolution	$\eta \times 10^4$	$\nu \times 10^4$	$u_{\rm rms}$	$b_{\rm rms}$	$P_{\rm M}$	$R_{\rm M}$
A	128^3	4.0	4.0	0.13	0.044	1	208
B	256^3	2.0	2.0	0.14	0.061	1	466
C	256^3	2.0	10.0	0.14	0.061	5	466
D	256^3	2.0	100.0	0.18	0.087	50	586
E	512^3	2.0	2.0	0.13	0.054	1	426
F	512^3	1.5	1.5	0.14	0.067	1	622
G	512^3	1.5	15	0.15	0.080	10	675

[2] To deduce a reasonable estimate for $R_{\rm M}$ usable in the simulation for a given grid size, we argue as follows: suppose we model $M(k)$ as a power law with $M(k) \propto k^s$. Then, an estimate of the maximum value of $R_{\rm M} = R_{\rm max}$ that can be obtained in a simulation with N mesh points is $R_{\rm max} \sim (k_{\rm f}/k_{\rm res})^{(s-1)/2}$, where $k_{\rm res} = N/2$ assuming that one needs to resolve the dissipation scale where $R_{\rm M}(k) = 1$ with at least three grid points. For Kolmogorov-like spectra, $s = -5/3$ and 512^3 box, the estimated $R_{\rm max}$ turns out to be $\sim$950. In all our runs, we focus on being able to resolve smaller scales, and thus conservatively do not exceed such estimates. Hence, for $P_{\rm M} > 1$ runs we increase the viscosity ν, thus reducing the fluid Reynolds numbers from the case of $P_{\rm M} = 1$.

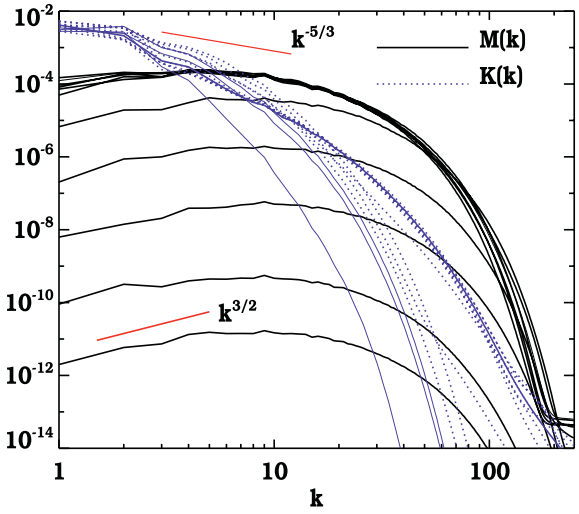

Figure 3. The time evolution of the kinetic $K(k)$ and magnetic spectra $M(k)$ for a 512^3 simulation of fluctuation dynamos with $R_M = 675$, $Re = 67.5$ (run G). The first time for the spectra is $45t_0$. The time difference between successive spectra is about ~ 23 eddy turnover times.

3 FARADAY ROTATION MEASURE FROM SIMULATIONS

The Faraday RM is defined as

$$\mathrm{RM} = K \int_L n_e \boldsymbol{B} \cdot \mathrm{d}\boldsymbol{l}, \tag{1}$$

where n_e is the thermal electron density, $\boldsymbol{B}$ is the magnetic field, the integration is along the LOS 'L' from the source to the observer and $K = 0.81$ rad m^{-2} cm^{-3} μG^{-1} pc^{-1}. In our simulations, as the motions are nearly incompressible, the density is almost constant throughout the box[3] (the rms density fluctuations are of the order of a few per cent), and one can take n_e out of the integral and denote it as $\bar{n}_e$. We have checked that inclusion of density in the integral to determine RM changes the result negligibly, by less than 1 per cent.

As in SSH, we directly compute, using the simulation data, $\int \boldsymbol{B} \cdot \mathrm{d}\boldsymbol{l}$, and hence the RM over $3N^2$ LOS, along each of the x-, y- and z-directions of the simulation box. For example, if the LOS integration is along z, at a given location (x_i, y_i), this involves a discrete sum of B_z of the form

$$\mathrm{RM}(x_i, y_i, t) = K\bar{n}_e \sum_{j=0}^{N-1} \left(\frac{2\pi}{N}\right) B_z\left(x_i, y_i, \frac{2\pi j}{N}, t\right). \tag{2}$$

As the random magnetic field produced by the fluctuation dynamo is expected to be nearly statistically isotropic, the mean value $\langle \int \boldsymbol{B} \cdot \mathrm{d}\boldsymbol{l} \rangle$ over all the LOS, and hence the mean RM are expected to nearly vanish. However, the rms value of RM, which we denote as σ_{RM}, will be non-zero.

It is also convenient to normalize the RM by the rms value expected in a simple model of the random magnetic fields. For example, consider a model where a field of strength B_{rms} fills each turbulent cell of scale $l = (2\pi/k_f)$ but is randomly oriented from one turbulent cell to another. Also suppose that the LOS of length L contains $M = L/l$ turbulent cells. In such a model, we expect the mean RM to vanish but its dispersion to be given by

$$\sigma_{\mathrm{RM0}} = K\bar{n}_e\, B_{\mathrm{rms}}\, l \left(\sum_{m,n=0}^{M-1} \langle \cos\theta_m \cos\theta_n \rangle\right)^{1/2}$$
$$= K\bar{n}_e \frac{B_{\mathrm{rms}}}{\sqrt{3}}\, l\sqrt{\frac{L}{l}} = K\bar{n}_e \frac{B_{\mathrm{rms}}}{\sqrt{3}} \left(\frac{2\pi}{k_f}\right)\sqrt{k_f}. \tag{3}$$

Here, θ_m is the angle between the LOS and the magnetic field in each cell, labelled by the index m. Also since θ_m's are independent and uniformly distributed over the solid angle, we have $\langle \cos\theta_m \cos\theta_n \rangle = \delta_{mn}/3$. Then only diagonal terms contribute to the sum, giving $\sum_{m,n} \langle \cos\theta_m \cos\theta_n \rangle = M/3 = (L/3l)$. Moreover, for the last equality in equation (3), we have replaced $l = 2\pi/k_f$ and taken $L = 2\pi$ the LOS length for the simulation box (see also SSH). Thus, the normalized RM defined as $\overline{\mathrm{RM}} = \mathrm{RM}/\sigma_{\mathrm{RM0}}$ is given by

$$\overline{\mathrm{RM}}(x_i, y_i, t) = \sum_{j=0}^{N-1} \left(\frac{2\pi}{N}\right) \frac{B_z(x_i, y_i, (2\pi j/N), t)}{B_{\mathrm{rms}}(t)(2\pi/k_f)\sqrt{k_f/3}} \tag{4}$$

for an LOS along the z-direction in the simulation box. This normalized RM is also expected to have a nearly zero mean, but a non-zero dispersion $\bar{\sigma}_{\mathrm{RM}}$. Due to the presence of $B_{\mathrm{rms}}(t)$ in the denominator, the normalized RM, $\bar{\sigma}_{\mathrm{RM}}$, will not grow if B_{rms} itself grows, but will only increase if the coherence scale of the field increases with time.

In order to determine $\bar{\sigma}_{\mathrm{RM}}$, we consider the cumulative distribution of the $\overline{\mathrm{RM}}$ for the N^2 LOS in each direction. Note that the cumulative distribution is preferred over the corresponding differential probability distribution function (PDF) to avoid uncertainties which arise due to the choice of the bin size. The cumulative probability distribution $C(X)$ can be determined by adding the number of occurrences of $\overline{\mathrm{RM}} > X$, starting at the lowest value in the data set, and normalizing by the total number N^2 of data points (to convert to probabilities). We show in Fig. 4 such a cumulative probability distribution $C(X)$ of $\overline{\mathrm{RM}}$ for the 512^3 simulation with $P_M = 1$ (run F), at $271t_0$, after the dynamo has saturated. We have chosen the LOS to be along the y-direction of the simulation box. The horizontal dotted lines show probability of the mean 0.5, and the 1σ levels of

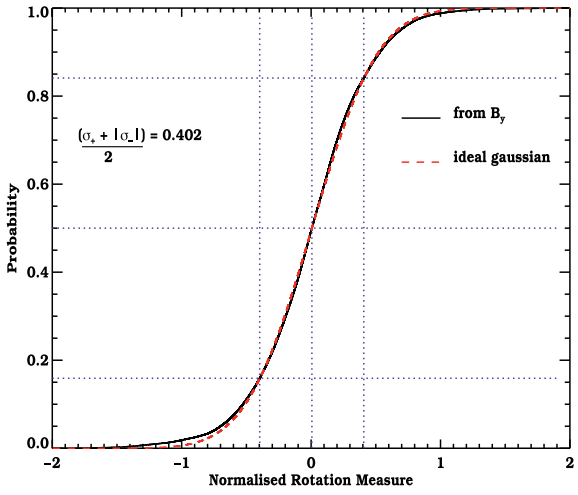

Figure 4. Cumulative probability distribution $C(x)$ of the normalized Faraday rotation measure $\overline{\mathrm{RM}}$ from run F at $t = 271t_0$. The horizontal lines show probability of the mean 0.5, and the 1σ levels of 0.159 and 0.841, assuming a Gaussian PDF. The vertical lines then indicate the corresponding mean $\langle\overline{\mathrm{RM}}\rangle$ and the $1\sigma_\pm$ values. Average between $|\sigma_\pm|$ is derived as 0.402. The cumulative PDF of a Gaussian distribution with a mean $\langle\overline{\mathrm{RM}}\rangle$ and the averaged 1σ value is also shown for comparison.

[3] Note that as the turbulent scales are much smaller than the system scale in general, n_e can still vary on scales larger than the scale of simulation box.

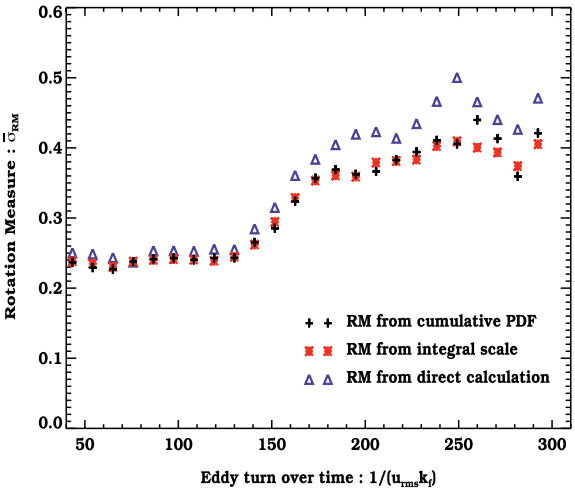

Figure 5. The time evolution of the normalized RM ($\bar{\sigma}_{\rm RM}$) for the 512^3 run (F), with $R_{\rm M} = Re = 622$. The crosses show the result of the direct calculation by shooting $3N^2$ LOS through the simulation box. The triangles show the result of the direct estimate of the standard deviation of RM, and the stars the result of integrating the energy spectrum (method III).

0.159 and 0.841, assuming a Gaussian PDF. The $\overline{\rm RM}$ values where these lines intersect the cumulative PDF $C(X)$ curve give then values of the corresponding mean $\langle\overline{\rm RM}\rangle$ and the dispersion σ_- and σ_+, respectively. For a Gaussian PDF with zero mean, we expect $\sigma_\pm$ to be equal and opposite, while for a general PDF their magnitudes can be different. We find the average dispersion, $(\sigma_+ + |\sigma_-|)/2$, and then define $\bar{\sigma}_{\rm RM}$ as its mean over all the three directions. We can also obtain a normalized RM dispersion by constructing a single cumulative PDF consisting of $\overline{\rm RM}$s from all the three directions. This matches closely with $\bar{\sigma}_{\rm RM}$ defined above. This is true for estimates made in both kinematic and saturated stages (we will refer to this method of estimating $\bar{\sigma}_{\rm RM}$ as method I). In the particular case shown in Fig. 4, we have the $\langle\overline{\rm RM}\rangle = 0.006$, $\sigma_+ = 0.401$, $\sigma_- = 0.403$ and the average dispersion $= 0.402$, obtained from the magnetic field in the y-direction. The average dispersions calculated from fields in the x- and z-directions are 0.464 and 0.366, respectively, giving therefore, $\bar{\sigma}_{\rm RM} = 0.411$ (as can be seen from Fig. 5). The cumulative PDF of a Gaussian distribution, with the same mean $\langle\overline{\rm RM}\rangle$ and dispersion (averaged 1σ value), is also shown for comparison. We see in this case that $C(X)$ is quite well fitted by the cumulative PDF of a Gaussian. Note that the components of B_i themselves are not expected to have a Gaussian PDF (Brandenburg & Subramanian 2005), but the RM involves a sum of B_i's over a large number of mesh points. The PDF of this sum would then tend to a Gaussian if the B_i's were independent or their correlation lengths were small compared to the box size, due to the central limit theorem.[4]

[4] An interesting feature that we find is that when only a part of the simulation box is considered for forming the cumulative PDF, its deviation from a Gaussian is large and $C(x)$ shows a large bias. One can in fact get $\overline{\rm RM}$ larger than $\bar{\sigma}_{\rm RM}$. This implies that the sampling of the entire turbulent cell is necessary to obtain a Gaussian cumulative PDF. Otherwise, when one is sampling only a part of the turbulent cell, correlated structures in the magnetic field can show up as a large bias in the PDF. Such a feature can be relevant in interpreting the RM observations, as in Murgia et al. (2004), where the radio source could be extended over a scale smaller than the turbulent scale.

There are other cases when the Gaussian PDF does not provide a good fit to the wings of $C(x)$. Thus, we also calculate for comparison $\bar{\sigma}_{\rm RM}$ directly as the standard deviation of the set of $\overline{\rm RM}(x_i, y_i, t)$ (henceforth method II). A third method (method III) of estimating $\bar{\sigma}_{\rm RM}$, which however assumes the statistical isotropy of the random magnetic field generated by the fluctuation dynamo, is to relate it to the integral scale of the field. We have using equation 9 of CR09 and equation (3) above

$$\bar{\sigma}_{\rm RM} = \frac{\sqrt{3}}{2}\sqrt{\frac{L_{\rm int}k_{\rm f}}{2\pi}} = \frac{\sqrt{3}}{2}\sqrt{\frac{L_{\rm int}}{l}}, \tag{5}$$

where $L_{\rm int}$ is the integral scale of the random magnetic field and is defined by

$$L_{\rm int}(t) = \frac{\int (2\pi/k)M(k,t)\,{\rm d}k}{\int M(k,t)\,{\rm d}k}. \tag{6}$$

Note that the integral scale as defined here has the same order of magnitude as the integral scales L_L and L_N defined, respectively, using the longitudinal and transverse correlation functions. For any statistically homogeneous, isotropic, reflection invariant and divergence-free vector field, $L_L = 2L_N = (3/8)L_{\rm int}$ (Monin & Yaglom 1975). Thus, given the magnetic power spectra $M(k, t)$, one can calculate the integral scale $L_{\rm int}(t)$ and hence the normalized RM, $\bar{\sigma}_{\rm RM}$. One can also see that for a fixed $k_{\rm f}$, the magnitude and evolution of $\bar{\sigma}_{\rm RM}$ essentially reflect the evolution of the integral scale $L_{\rm int}$. This method is useful for estimating $\bar{\sigma}_{\rm RM}$ from just the magnetic spectra, assuming statistical isotropy; however, it cannot be used to separate the $\bar{\sigma}_{\rm RM}$ contribution from high-field structures versus the general volume filling field (see below). We now turn to the results of the computations of $\bar{\sigma}_{\rm RM}$ for the various simulations that we have performed and their implications.

4 RM FROM FLUCTUATION DYNAMOS: RESULTS

We begin by considering one of the runs of fluctuation dynamos with the highest value of $R_{\rm M}$, run F, with 512^3 resolution and $Re = R_{\rm M} = 622$. The time evolution of the normalized RM, $\bar{\sigma}_{\rm RM}(t)$, for this run is shown in Fig. 5, starting from the kinematic stage to the saturation of the dynamo. The results are shown for all three methods of calculating $\bar{\sigma}_{\rm RM}$. The crosses show the result of calculating RM by shooting $3N^2$ LOS through the simulation box (method I), the triangles the direct estimate of the standard deviation of $\overline{\rm RM}$ (method II) and the stars the result of integrating the energy spectrum (method III).

First, we find that all three estimates of $\bar{\sigma}_{\rm RM}$ agree reasonably well, closer agreement being obtained between methods I and III. The agreement between method I, which uses a configuration space analysis, and method III using the Fourier space spectrum is reassuring. The direct estimate of the standard deviation (method II) also agrees with the other methods at early times, but later as the dynamo saturates, it always gives a larger estimate of $\bar{\sigma}_{\rm RM}$ by about 10–20 per cent. This indicates that after saturation, there is usually an excess of $\overline{\rm RM}$ in the wings of the cumulative PDF over and above that predicted by a Gaussian approximation to $C(X)$. This excess could arise due to the increase in the magnetic correlation scale and the deviation from statistical isotropy when the dynamo saturates.

We see from Fig. 5 that the normalized Faraday RM is almost constant in the kinematic stage with $\bar{\sigma}_{\rm RM} \sim 0.24$. This is obtained even though $B_{\rm rms}$ itself is growing exponentially. It indicates that during the kinematic stage, the spectrum $M(k, t)$ evolves in a

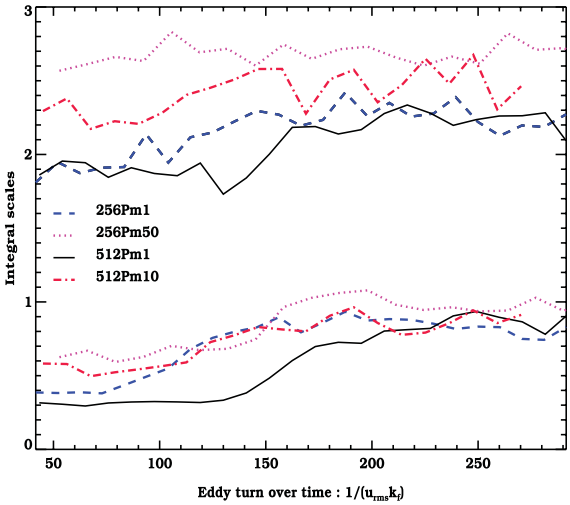

Figure 6. Comparison of integral scale for runs B, D, F and G. The lines on the upper half of the plot correspond to the velocity integral scales, $L_{\rm int}^{V}$, and those on the lower half correspond to the magnetic integral scales, $L_{\rm int}$. The line styles are matched with those in Fig. 1 to be able to compare the times at which the integral scales start growing to the corresponding regime in the magnetic field growth.

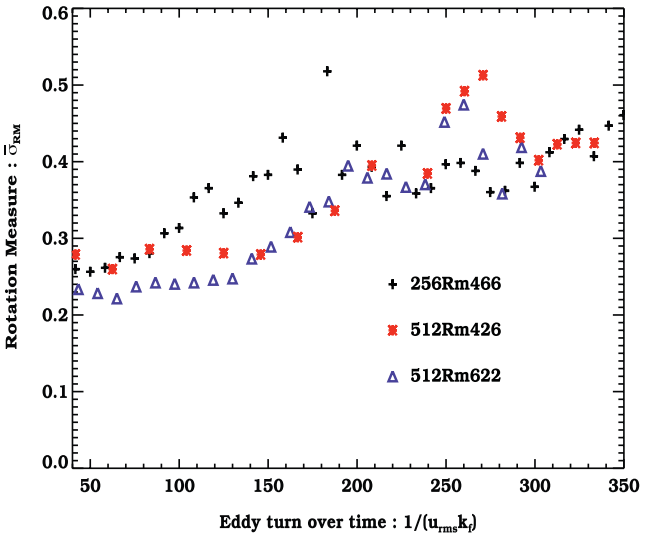

Figure 7. Sensitivity of RM to $R_{\rm M}$. The time evolution of $\bar{\sigma}_{\rm RM}$ calculated using method I is shown for simulations (runs B, E, F) with different $R_{\rm M}$ keeping $P_{\rm M} = 1$.

self-similar fashion, maintaining the integral scale. However, by the time the dynamo saturates, there is a substantial increase in the normalized RM to the value $\bar{\sigma}_{\rm RM} \sim 0.4{-}0.5$. Since $\bar{\sigma}_{\rm RM}^2$ is directly proportional to the integral scale $L_{\rm int}$ (in method III), this implies that $L_{\rm int}$ has increased by a factor of ∼3 as one goes from the kinematic to the saturated state. To check this, we have shown in Fig. 6, the time evolution of both the magnetic and kinetic integral scales for various runs. We can see that for the $P_{\rm M} = 1, R_{\rm M} = 622$ run, $L_{\rm int}$ does increase from a value of about 0.3 in the kinematic stage to $L_{\rm int}$ ∼ 0.9, or a factor of ∼3, by the time the dynamo saturates (see the thick solid line at the bottom of Fig. 6). In contrast, we find that the corresponding integral scale of the velocity field $L_{\rm int}^{V}$ [defined as in equation (6) with $M(k)$ replaced by $K(k)$] only grows from about 2 to a value of 2.2 during the same period (the black solid line in the upper half of Fig. 6).

Importantly, a comparison of Figs 5 and 6 with Fig. 1 shows that the magnetic integral scale and the $\bar{\sigma}_{\rm RM}$ begin to increase at $t/t_0 \sim$ 150 just as the field begins to saturate due to the influence of Lorentz forces. In fact, a comparison of Figs 6 and 1 shows that for all the cases we have considered, the magnetic integral scale increases when Lorentz forces become important, whereas the integral scale of the velocity field changes very little during this period. Thus, clearly, it is the influence of the Lorentz forces that leads to larger and larger coherence scale of the magnetic field reflected in the increase of $L_{\rm int}(t)$ and $\bar{\sigma}_{\rm RM}$.

The value of $\bar{\sigma}_{\rm RM} \sim 0.4$–$0.5$ that we obtain is quite significant given that one expects the fluctuation dynamo generated field to be fairly intermittent. It implies that the rms value of RM in the saturated state of the fluctuation dynamo is of the order of 40–50 per cent of that expected in a model where $B_{\rm rms}$ strength fields volume fill each turbulent cell, but are randomly oriented from one cell to another. We will apply this result in Section 5 to discuss the RM obtained in various astrophysical systems.

4.1 Sensitivity of RM to $R_{\rm M}$ and $P_{\rm M}$

It is important to test the sensitivity of the RM produced by the fluctuation dynamo generated fields to changes in the values of the magnetic Reynolds number and Prandtl number. For testing the sensitivity of our results to $R_{\rm M}$, we have run another high-resolution (512^3) simulation with a lower $R_{\rm M} = 426$ and $P_{\rm M} = 1$ (run E) to compare with run F, where $R_{\rm M} = 622$. The results of RM analysis for both these simulations are compared in Fig. 7, where we plot the time evolution of $\bar{\sigma}_{\rm RM}$ obtained from these runs. To check the effect of the resolution, we also show in the figure the results from a 256^3 run having a similar $R_{\rm M} = 466$ (run B). We see that $\bar{\sigma}_{\rm RM}$ for the lower $R_{\rm M}$ runs starts off with a higher value in the kinematic stage as expected, if the integral scale is initially larger. Such an expectation is consistent with what is seen in Fig. 6 (compare the black solid and blue dashed lines). The reason for this larger $L_{\rm int}$ in the kinematic stage is probably that only slightly larger scale eddies are able to amplify the field (these are the eddies for which $R_{\rm M}(k)$ defined as $u_{\rm rms}(k)/k\eta$ or $\sqrt{kK(k)}/k\eta$ is greater than $R_{\rm crit}$) in the lower $R_{\rm M}$ cases, compared to the case when $R_{\rm M} = 622$ (see also the discussion below of Fig. 10).

Again as the field begins to saturate, $\bar{\sigma}_{\rm RM}$ increases due to the ordering effect of Lorentz forces, and asymptotes to a value between 0.4 and 0.5, for runs B and E as well. It is of interest to note that for run B where the Lorentz forces become important at an earlier time compared to runs F and E, the rise of $\bar{\sigma}_{\rm RM}$ also begins earlier. Our results are thus consistent with the idea that $\bar{\sigma}_{\rm RM}$ obtained in the saturated state is independent of $R_{\rm M}$, although we have explored at present only a modest range of $R_{\rm M}$.

It is of interest to compare our results with that obtained from an independent $R_{\rm M} = 1784$, $P_{\rm M} = 1$, 1024^3 simulation of the fluctuation dynamo whose data are publicly available online at the Johns Hopkins University (JHU) turbulent data base (Perlman et al. 2007; Li et al. 2008). These authors simulate the fluctuation dynamo using a forcing in the form of a Taylor–Green flow with $k_{\rm f} = 2$. They give the integral scales of the velocity and magnetic fields in the saturated state of the dynamo to be $L_{\rm int}^{V} = 1.5$ and $L_{\rm int} = 0.93$, respectively (in our definition). We can use these data in equation (5) to estimate the $\bar{\sigma}_{\rm RM}$. We get $\bar{\sigma}_{\rm RM} = 0.47$, which is remarkably consistent with our results above. As this is an independent simulation with a much higher $R_{\rm M}$, it would appear that $\bar{\sigma}_{\rm RM} \sim 0.4{-}0.5$ is a robust result, at least for the $P_{\rm M} = 1$ case.

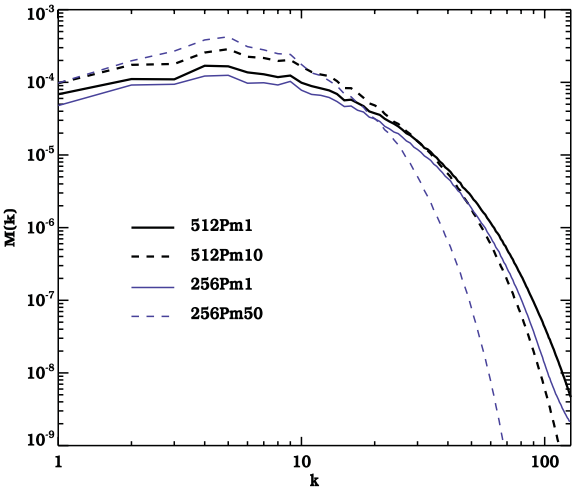

Figure 8. Comparison of the final saturated magnetic spectra from different P_M runs (B, D, E and F).

In order to test the sensitivity of our results to having higher P_M, we have also run a suite of simulations with the same resolution (256^3), but with varying $P_M = 1, 5, 50$ (runs B, C, D), and also one with a higher resolution (512^3) with $P_M = 10$ (run G) (note that in galactic and cluster plasmas, one expects $P_M \gg 1$). In contrast to Schekochihin et al. (2004), we have increased P_M by increasing the viscosity ν (decreasing Re), while keeping the resistivity constant across runs. This is in keeping with the needed resolution at small scales, as explained in Section 2 (we have nevertheless kept $Re \gg 1$ for all the runs). Interestingly, when Re is decreased keeping R_M almost the same (so as to increase P_M), we find that the magnetic spectra in the saturated state seem to have lower energy at the small 'resistive' scales for a larger P_M; see Fig. 8.

In the top panel of Fig. 9, we show the time evolution of $\bar{\sigma}_{RM}$ for the runs with 256^3 resolution. We also show the $\bar{\sigma}_{RM}$ evolution for the higher resolution runs with $P_M = 1$ and 10 separately in the bottom panel. In the kinematic stage, we find that $\bar{\sigma}_{RM}$ tends to be larger for higher P_M, but it also tends to be smaller for higher

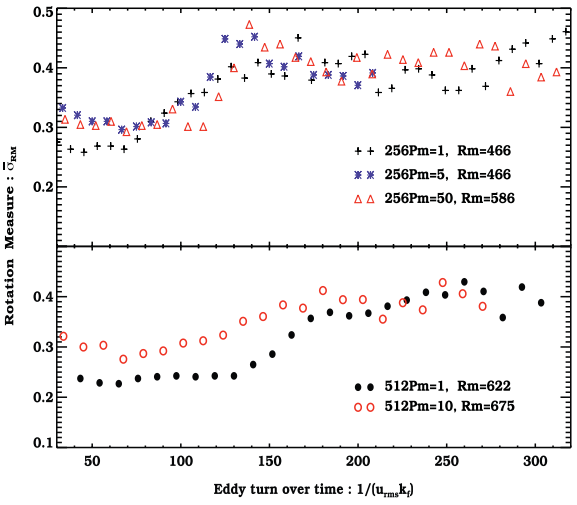

Figure 9. Sensitivity of RM to P_M. The top panel shows time evolution of $\bar{\sigma}_{RM}$ for simulations with different $P_M = 1, 5, 50$, for runs (B, C and D) having the same resolution, 256^3. The bottom panel shows time evolution of $\bar{\sigma}_{RM}$ (using method I) for simulations of higher resolution 512^3, with $P_M = 1$ and 10 (runs F and G).

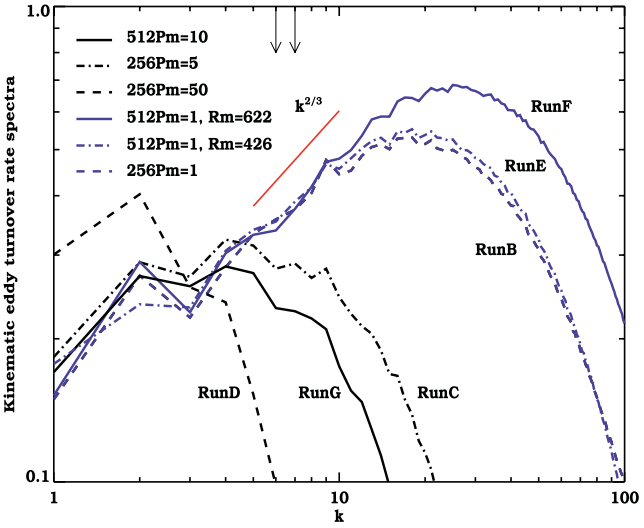

Figure 10. Comparison of the eddy turnover rate spectra from different runs, in the kinematic stage. Spectra are plotted at $t \sim 83t_0$ for run B, $t \sim 64t_0$ for run C, $t \sim 80t_0$ for run D, $t \sim 43t_0$ for run F and $t \sim 45t_0$ for run G.

R_M. This again basically reflects the corresponding dependence of the magnetic integral scale on these parameters (see Fig. 6). The integral scale of the velocity field itself (shown in Fig. 6) is expected to be larger for the larger P_M case (assuming the same forcing scale), since a larger viscosity (for the high-P_M run) damps more of the small-scale power in the velocity field.

In order to understand the reason for a larger magnetic integral scale in the kinematic stage for the higher P_M run, it is instructive to look also at Fig. 10. Here we have given the spectra of eddy turnover rate defined as $\gamma(k) = k\sqrt{kK(k)}$ at times when the dynamo is still in the kinematic stage. We see that $\gamma(k)$ rises with k till about $k \sim 25$ for the run F with $P_M = 1$. While for run G with $P_M = 10$, $\gamma(k)$ is maximum and relatively flat in the range $k \sim 2-5$. Note that eddies with a scale such that $\gamma(k)$ is larger will tend to grow the field first, provided their corresponding magnetic Reynolds number $R_M(k)$ is supercritical. For run F, this happens for k smaller than a critical value $k_{crit} = 7$, while for runs B, E and G, $k_{crit} = 6$ (we have marked the k_{crit} for these runs by arrows in Fig. 10). Since such eddies have a smaller k for the $P_M = 10$ run compared to the $P_M = 1$ case, we do expect a larger L_{int} for the former case compared to the latter, during the kinematic evolution.

On the other hand, as can be seen from Fig. 9, the value of $\bar{\sigma}_{RM}$ in the saturated state is very similar for all the runs we have considered. In particular, we again obtain $\bar{\sigma}_{RM} = 0.4-0.45$ (from method I) in the saturated state, independent of P_M, R_M and the resolution of the run. Moreover, in all cases, as also discussed earlier, the start of an increase in $\bar{\sigma}_{RM}$ and L_{int} from their values in the kinematic stage is associated with the onset of saturation due to Lorentz forces.

We have summarized the results of the RM computation for all the runs in Table 2. Looking at the last two columns of the table, we find that $\bar{\sigma}_{RM} \sim 0.4-0.5$ is obtained in the saturated state of the fluctuation dynamo almost universally. It thus appears from our work that the effect of Lorentz force is to order the field to a maximum scale which only depends on the forcing scale, but is independent of the P_M and R_M. It would be important to do even higher R_M and P_M simulations in the future to firm up these conclusions.

Table 2. Summary of the results obtained from various simulation runs. The individual integral scale values are obtained by averaging the results over each stage (kinematic and saturated), where the evolution curves are relatively flat (i.e. the period where these scales increase is not considered for averaging). Similarly, the $\bar{\sigma}_{\rm RM}$ values are obtained by averaging the results over the saturated stage. The independent JHU simulation (1024^3) result has also been shown in the last row for comparison. Note that the forcing scale is $k_{\rm f} = 2$ for their run.

				Kinematic		Saturation		$\bar{\sigma}_{\rm RM}$	
Run	Res	$P_{\rm M}$	$R_{\rm M}$	$L_{\rm int}$	$L^V_{\rm int}$	$L_{\rm int}$	$L^V_{\rm int}$	PDF	Direct
A	128^3	1	208	1.0	2.8	1.2	2.8	0.41	0.50
B	256^3	1	466	0.4	1.9	0.8	2.2	0.41	0.46
C	256^3	5	466	0.6	2.2	0.9	2.5	0.39	0.46
D	256^3	50	586	0.6	2.6	1.0	2.7	0.41	0.49
E	512^3	1	426	0.4	2.0	1.0	2.0	0.45	0.49
F	512^3	1	622	0.3	1.9	0.9	2.2	0.41	0.46
G	512^3	10	675	0.5	2.2	0.8	2.5	0.39	0.44
JHU	1024^3	1	1784			0.93	1.5		0.47

4.2 Introducing cutoffs

The fluctuation dynamo generated fields are seen to be fairly intermittent, especially if one looks at the high-field regions (HBD; Schekochihin et al. 2004; Brandenburg & Subramanian 2005). An interesting question is to what extent the RM produced by such a field arises in high-field structures compared to the less intense volume filling field regions. Addressing this issue could be important, in case the high-field regions are sensitive to $R_{\rm M}$ and $P_{\rm M}$. Thus, it is useful to distinguish the RM contribution from regions with differing field strengths. Note that this can only be done from an actual realization of the fluctuation dynamo generated field, and not by having only the information about the magnetic power spectrum.

We therefore calculate RM along each LOS, now leaving out regions where the field satisfies the constraint $B^2 = (B_x^2 + B_y^2 + B_z^2) > (nB_{\rm rms})^2$, with $n = 1$ and 2. We repeat the same exercise of calculating the cumulative PDF, $C(X)$, at each time and finding the $\bar{\sigma}_{\rm RM}$ after imposing the above constraint. Fig. 11 shows the results

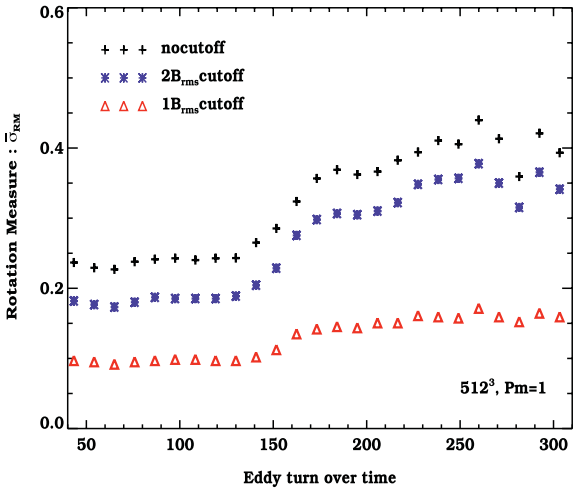

Figure 11. The time evolution of the normalized RM ($\bar{\sigma}_{\rm RM}$) for the 512^3 run (F), determined excluding the regions with $|\boldsymbol{B}| > nB_{\rm rms}$. The crosses correspond to not imposing any cutoff, the stars show the result of excluding $|\boldsymbol{B}| > 2B_{\rm rms}$ regions, while the triangles show the result of excluding regions with $|\boldsymbol{B}| > B_{\rm rms}$.

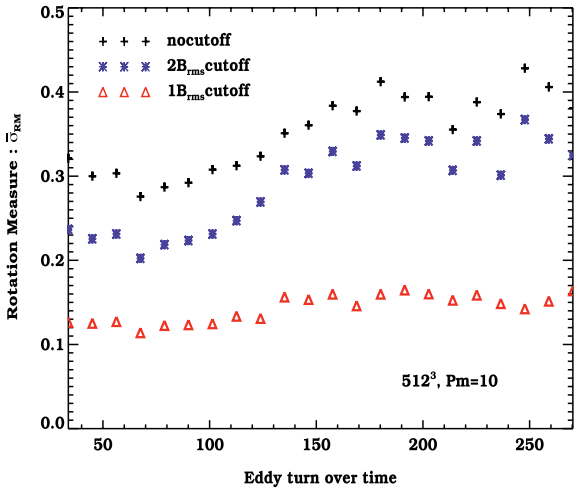

Figure 12. The time evolution of the normalized RM ($\bar{\sigma}_{\rm RM}$) for the 512^3, $P_{\rm M} = 10$ run (G), determined excluding the regions with $|\boldsymbol{B}| > nB_{\rm rms}$. The crosses correspond to not imposing any cutoff, the stars show the result of excluding $|\boldsymbol{B}| > 2B_{\rm rms}$ regions, while the triangles show the result of excluding regions with $|\boldsymbol{B}| > B_{\rm rms}$.

for the $P_{\rm M} = 1$ run F, while Fig. 12 shows corresponding results for the $P_{\rm M} = 10$ run with 512^3 resolution (run G). The crosses in Figs 11 and 12 correspond to not imposing any cutoff, the stars show the result of excluding $B > 2B_{\rm rms}$ regions, while the triangles show the result of excluding regions with $B > B_{\rm rms}$. The time evolution of $\bar{\sigma}_{\rm RM}$ is shown right from the kinematic stage up into saturation.

We find that $\bar{\sigma}_{\rm RM}$ with a $B > 2B_{\rm rms}$ cutoff has a similar time evolution to the case with no cutoff, but with a reduced amplitude. From Fig. 11, for the $P_{\rm M} = 1$ case, one finds that the regions with a field strength larger than $2B_{\rm rms}$ contribute only 15–20 per cent to the total RM. Thus, the reduction in the RMs calculated after one cuts off the $2B_{\rm rms}$ fields is quite small. On the other hand, if one removes regions with a field strength larger than $1B_{\rm rms}$, then the RM decreases substantially, by a factor of 3 or so. Moreover, the reduction in the RM with a cutoff is almost the same, right from the kinematic stage to the saturated state. This perhaps goes to show that the fields generated by the $P_{\rm M} = 1$ fluctuation dynamo grow in a self-similar manner and the configurations do not change on the average substantially from the kinematic stage to saturation.

For the $P_{\rm M} = 10$ case shown in Fig. 12, we find that the regions with a field strength larger than $2B_{\rm rms}$ contribute 25 per cent to the total RM in the kinematic stage. However, their contribution reduces to about 15 per cent in the saturation stage, similar to the $P_{\rm M} = 1$ case. Again then the RM decreases substantially, by a factor of 3 if one removes regions with a field strength larger than $1B_{\rm rms}$.

These results thus show for both cases that the general 'sea' of volume filling fluctuating fields contribute dominantly to the RM produced by the fluctuation dynamo, rather than the high-field regions, right from the kinematic stage to the saturated state.

5 ASTROPHYSICAL APPLICATIONS

An important application of the above results is to galaxy cluster plasma and their magnetic fields as inferred from radio observations (Clarke et al. 2001; Carilli & Taylor 2002; Govoni & Feretti 2004; Murgia et al. 2004; Vogt & Enßlin 2005; Bonafede et al. 2010, 2011; Govoni et al. 2010; Vacca et al. 2010; Kuchar & Enßlin 2011). Note that the cluster magnetic fields will decay if not maintained by a turbulent dynamo of the nature considered in this work. As

mentioned in the introduction, there is considerable evidence from both observations and cosmological simulations that cluster turbulence is nearly incompressible. Thus, our simulation results are directly applicable in the context of explaining cluster magnetism.

Given the $\bar{\sigma}_{\rm RM}$ obtained in our simulations, one can estimate the expected dispersion of the RM, $\sigma_{\rm RM}$, in any given astrophysical system. This is given by

$$\begin{aligned}\sigma_{\rm RM} &= \bar{\sigma}_{\rm RM}\, K\, \bar{n}_{\rm e}\, \frac{B_{\rm rms}}{\sqrt{3}}\, l\sqrt{\frac{L}{l}}\ {\rm rad\ m^{-2}} \\ &= 180\ {\rm rad\ m^{-2}} \left(\frac{\bar{\sigma}_{\rm RM}}{0.4}\right) \left(\frac{\bar{n}_{\rm e}}{10^{-3}\ {\rm cm^{-3}}}\right) \left(\frac{B_{\rm rms}}{3\ \mu{\rm G}}\right) \\ &\quad \times \left(\frac{l}{100\ {\rm kpc}}\right)^{1/2} \left(\frac{L}{1\ {\rm Mpc}}\right)^{1/2}. \end{aligned} \tag{7}$$

For obtaining a numerical estimate of $\sigma_{\rm RM}$, we have adopted average values of various parameters appropriate for a galaxy cluster (see below).

In order to estimate $B_{\rm rms}$ for the fluctuation dynamo generated field, we note from Table 1 that on saturation the fluctuation dynamo generated field grows to a value of $B_{\rm rms} \sim u_{\rm rms}/2$, in dimensionless code units. Therefore, $B_{\rm rms} \sim B_{\rm eq}/2$ on saturation, where $B_{\rm eq} = \sqrt{4\pi\rho u_{\rm rms}^2}$ is the field strength which is in equipartition with the turbulent motions. This is given by

$$B_{\rm eq} = 6.1\ \mu{\rm G} \left(\frac{n}{10^{-3}\ {\rm cm^{-3}}}\right)^{1/2} \left(\frac{u_{\rm rms}}{300\ {\rm km\ s^{-1}}}\right), \tag{8}$$

where we have used $n = \rho/m_p$.

For a galaxy cluster, $n = n_{\rm e} \sim 10^{-3}\ {\rm cm^{-3}}$, $u_{\rm rms} \sim 200$–$300\ {\rm km\ s^{-1}}$, $l \sim 100$ kpc and $L \sim 1$ Mpc (cf. SSH and references therein). The eddy turnover time at the forcing scale is $\tau \sim l/u_{\rm rms} \sim 3 \times 10^8$ yr. This τ is short compared to the cluster age or the time-scale for which mergers can sustain turbulence (SSH; Ryu et al. 2012). Therefore, magnetic fields are likely to be amplified to the saturation value by the fluctuation dynamo. One may then expect $B_{\rm eq} \sim 4$–$6\ \mu$G, and a fluctuation dynamo generated field with $B_{\rm rms} \sim 2$–$3\ \mu$G in a galaxy cluster. Then equation (7) predicts an rms value of RM, $\sigma_{\rm RM} \sim 120$–$180\ {\rm rad\ m^{-2}}$ in galaxy clusters. The data presented by Clarke et al. (2001) show a typical scatter in the RM values for LOS through galaxy clusters of $\sim 100\ {\rm rad\ m^{-2}}$. Therefore, one sees that the average value of $\bar{\sigma}_{\rm RM}$ obtained from our simulation of the fluctuation dynamo is sufficiently large to account for the RM measured in galaxy clusters.

The above average estimates can be generalized to the situation where the $n_{\rm e}$ and $B_{\rm rms}$ depend on the cluster radius. We have considered this in detail in Appendix A. Assuming that the correlation scale of the turbulence is small compared to the cluster scales, it turns out that this simply involves replacing $\bar{n}_{\rm e}^2 B_{\rm rms}^2 L$ in equation (7), when squared, by the integral I, given by

$$I(\boldsymbol{r}_\perp) = \int n_{\rm e}^2(\boldsymbol{r}_\perp, Z) B_{\rm rms}^2(\boldsymbol{r}_\perp, Z)\, {\rm d}Z, \tag{9}$$

where the LOS is parallel to the Z-direction and $\boldsymbol{r}_\perp$ is the perpendicular displacement from the centre of the cluster. Then the $\sigma_{\rm RM}$ for such a model is given by equation (A3), which after using $L_L = 3L_{\rm int}/8$ and $L_{\rm int} = 4\,\bar{\sigma}_{\rm RM}^2 l/3$ from equation (5) can be written as

$$\sigma_{\rm RM}^2 = \bar{\sigma}_{\rm RM}^2\, \frac{K^2\, l}{3}\, I\ {\rm rad\ m^{-2}}. \tag{10}$$

Using the standard β-model for the density profile of a cluster, $n_{\rm e} \propto (1 + r^2/r_{\rm c}^2)^{-3\beta/2}$ ($r_{\rm c}$ is the cluster core radius) and assuming $B_{\rm rms} \propto n_{\rm e}^\gamma$, we can evaluate the integral, I, exactly (see Appendix A). We get

$$\sigma_{\rm RM}(r_\perp) = \sigma_{\rm RM}(0) \left(1 + \frac{r_\perp^2}{r_{\rm c}^2}\right)^{-\frac{(6\beta(\gamma+1)-1)}{4}}, \tag{11}$$

where

$$\sigma_{\rm RM}(0) = \bar{\sigma}_{\rm RM} \frac{\pi^{1/4}}{\sqrt{6}}\, K n_0 B_0 \sqrt{r_{\rm c}\, l}\, \sqrt{\frac{\Gamma(3\beta(\gamma+1)-0.5)}{\Gamma(3\beta(\gamma+1))}} \tag{12}$$

and n_0, B_0 are the central density and rms magnetic field strength, respectively.

As an example, consider the Coma cluster, where we adopt from Bonafede et al. (2010), $n_0 = 3.44 \times 10^{-3}{\rm cm^{-3}}$, $\beta = 0.75$, $r_{\rm c} = 291$ kpc and a constrained $B_0 = 3.9\ \mu$G for $\gamma = 0.4$. For these values, and assuming $l = 100$ kpc, the $\sigma_{\rm RM}$ for a source seen through the Coma cluster at an impact parameter distance, $r_\perp = 50$ kpc, is estimated to be $\sigma_{\rm RM} \sim 310\ (\bar{\sigma}_{\rm RM}/0.4)\ {\rm rad\ m^{-2}}$, which is close to the value $\sigma_{\rm RM,obs} = 303\ {\rm rad\ m^{-2}}$ observed, as quoted in Bonafede et al. (2010). Note that this crucially depends on the normalized $\bar{\sigma}_{\rm RM}$ or the magnetic field correlation scale as determined from the fluctuation dynamo simulations being large enough, which we have shown here is indeed the case. Importantly, for the case of Coma, Bonafede et al. (2010) also note that the magnetic field as determined from RM measurements averaged over a Mpc^3 volume is compatible with equipartition estimates obtained from modelling the Coma radio halo. Thus for the case of Coma, a picture whereby magnetic fields are amplified by a fluctuation dynamo driven by incompressible turbulence seems consistent with radio observations.

The fluctuation dynamo can also lead to magnetic field generation in intergalactic filaments at the present epoch. Here, vorticity and turbulence are generated in shocks resulting from large-scale structure formation (Ryu et al. 2008, 2012; Iapichino et al. 2011). Combining the estimated levels of the resulting turbulence with a model of magnetic field generation by the fluctuation dynamos, Ryu et al. (2008) and CR09 estimate a magnetic field of tens of nG in these filaments and their RM contribution to be $\sim 1\ {\rm rad\ m^{-2}}$. A crucial question is again, how coherent is the dynamo generated field, which has been the focus of our work.

Consider now the case of the ISM of a gas-rich disc galaxy, possibly at high redshift. In galaxies SNe typically drive the turbulence, and even though the forcing may be largely compressible and at high mach numbers, the intersection of shocks and shock propagation through the inhomogeneous ISM lead to vorticity generation. The resulting vortical turbulent motions can again drive a fluctuation dynamo and amplify magnetic fields (Korpi et al. 1999; Haugen, Brandenburg & Mee 2004b; Balsara & Kim 2005; de Avillez & Breitschwerdt 2005; Gressel et al. 2008; Wu et al. 2009; Federrath et al. 2011; Gent et al. 2012). Note that if a gas mass $M \sim 10^{10}\ {\rm M_\odot}$ is distributed in a disc of radius $r = 10$ kpc and thickness $2h = 1$ kpc, the average density is $n \sim 1.4\ {\rm cm^{-3}}$. For example, the total stellar mass in our Galaxy is $\sim 6 \times 10^{10}\ {\rm M_\odot}$ (Binney & Tremaine 1987) and the gas mass could be about 10 per cent of this value. For such a galaxy, one would get $n \sim 0.84\ {\rm cm^{-3}}$. One may have a higher gas mass fraction for a high-redshift disc galaxy. We adopt $n = 1\ {\rm cm^{-3}}$ to estimate $B_{\rm eq}$. A caveat is that the turbulence in the ISM is expected to be transonic. In principle, for such turbulence, density fluctuations correlated with the field could affect the RM estimates. However, several simulations of SN-driven turbulence do not find a very strong correlation between magnetic field and density (de Avillez & Breitschwerdt 2005; Wu et al. 2009) and so, we expect our RM estimates to be reasonably indicative.

Let us adopt a typical vortical turbulent velocity of $u_{\rm rms} \sim 10$ km s^{-1} of the order of the sound speed in the warm ionized ISM, and a turbulent forcing scale of $l \sim 100$ pc (Korpi et al. 1999; Shukurov 2004). Then the eddy turnover time $\tau \sim 10^7$ yr is much less that the age of disc galaxies, even at high redshifts. Thus, one expects the fluctuation dynamo to grow the magnetic field to saturation even for weak seed fields. This then gives $B_{\rm eq} \sim 6.5$ μG and $B_{\rm rms}$ could be a fraction f of this value. For an LOS of length $L = 1$ kpc through the disc thickness, and $f \sim 1/2$, we get from equation (7), $\sigma_{\rm RM} \sim 180$ rad m^{-2}. Thus, again, significant Faraday rotation is expected if an LOS from a background radio source passes through a gas-rich disc galaxy, even if the fields produced in such a disc are purely through fluctuation dynamo action. In other words, observations of significant RM at high redshift need not require the canonical mean-field helical dynamo to have generated large-scale coherent fields. We emphasize that these results are only indicative and one requires much more work on fluctuation dynamo action in SN-driven turbulence to substantiate the above conclusions. It is also perhaps worth noting that significant magnetic field generation could occur even before forming the disc, due to the fluctuation dynamo action in the turbulent halo gas as the galaxy forms, in a manner similar to what we have discussed in cluster plasma (Kulsrud et al. 1997; Arshakian et al. 2009; Schleicher et al. 2010; Beck et al. 2012; Schober et al. 2012; Sur et al. 2012). Again whether this produces coherent enough fields is the crucial issue, one which we have answered in the affirmative in our work here.

Note that only some of the Mg II absorption systems probed by Bernet et al. (2008) are likely to arise in LOS through a galaxy disc. It is believed that many of these LOS could also be sampling the gaseous halo around a massive galaxy (cf. the review by Churchill, Kacprzak & Steidel 2005) or even an associated smaller dwarf galaxy only detected by spectral stacking (Noterdaeme, Srianand & Mohan 2010). The halo gas is likely to be hot, either accreted during the formation of the galaxy or transported out of the disc in an SN-driven wind or fountain flow (see for example Nestor et al. 2011; Bouché et al. 2012). This halo medium needs to contain not only the hot gas but also entrained magnetized cool gas which produces both the Mg II absorption and the excess RM seen by Bernet et al. (2008). Alternatively, the much cooler and magnetized material could be driven out by the pressure of cosmic rays as in the wind models of Samui, Subramanian & Srianand (2010). We are assuming here that the magnetization of the gas takes place in the disc by say the fluctuation dynamo, and then this gas is ejected in the wind, along with the metals. Alternatively, if the hot wind is turbulent, then the fluctuation dynamo can operate in the wind itself.

We model such Mg II systems by assuming say that the LOS through the gaseous halo passes through M magnetized (and Mg II rich) 'clouds' each of scale l, electron density $\bar{n}_{\rm e}$ and with an average field of strength B_0, which is again randomly oriented from cloud to cloud. Then an analysis identical to that which gave equation (3) can be applied. The resulting rms value of RM, $\sigma_{\rm RM}$, through such an LOS will be given by

$$\sigma_{\rm RM} = K \bar{n}_{\rm e} \frac{B_0}{\sqrt{3}} l \sqrt{M} = K N_{\rm e} \frac{B_0}{\sqrt{3M}} = \frac{160}{\sqrt{M}} \text{ rad m}^{-2} \left(\frac{N_{\rm e}}{10^{20} \text{ cm}^{-2}} \right) \left(\frac{B_0}{10 \, \mu\text{G}} \right). \quad (13)$$

Here, $N_{\rm e} = (\bar{n}_{\rm e} l) M$ is the total electron column density through the M magnetized clouds. The magnetic field in a cloud, which is denser than the average ISM, could be larger than the $B_{\rm rms}$ estimated from fluctuation dynamo action in the average density ISM. For example, if the cloud density is 10 times larger (like say a compact H II region in the ISM), then assuming flux freezing, $B_0 \sim 10^{2/3} B_{\rm rms} \sim 15$ μG. Bernet et al. (2008) estimate $N_{\rm e} \sim 10^{20}$ cm^{-2} for their Mg II systems, while the multiplicity of components M will vary from system to system. Then adopting $B_0 \sim 5$–15 μG, we see from equation (13) that $\sigma_{\rm RM} \sim (80\text{–}230)/\sqrt{M}$ rad m^{-2}. This will be within about the 1σ value inferred by Bernet et al. (2008), who find $\sigma_{\rm RM} \sim 140^{+80}_{-50}$ rad m^{-2}, for $M < 7$. Thus, the level of RM excess detected in the Mg II systems seems marginally consistent with theoretical expectations.

6 DISCUSSIONS AND CONCLUSIONS

There is considerable evidence for the presence of coherent magnetic fields in various astrophysical systems from galaxies to galaxy clusters. Much of this evidence comes from measurements of Faraday rotation. These systems are also generically turbulent and would therefore host what are referred to as fluctuation or small-scale dynamos. Such a dynamo amplifies magnetic fields on the fast eddy turnover time-scales. However, the generated fields are believed to be intermittent. We have considered whether the fluctuation dynamo generated fields can nevertheless lead to a sufficient degree of Faraday rotation so as to explain the observations. This is especially important for systems which are either too young or do not have the required conditions, for significant amplification of the field by a large-scale dynamo.

For this purpose, we have run a suite of fluctuation dynamo simulations in periodic boxes, with resolutions of up to 512^3, and for a range of $R_{\rm M}$ and $P_{\rm M}$. We can then directly calculate the time evolution of the Faraday RM predicted by these simulations from the kinematic to the saturated state of the fluctuation dynamo. We have used three different methods for this purpose. In the first method (I) we shoot $3N^2$ LOS through the simulation box, form cumulative PDFs of the measured RMs and estimate its normalized dispersion $\bar{\sigma}_{\rm RM}$, as the 1σ range contains the central 68.2 per cent of RM values. We have also directly calculated the standard deviation of the measured RMs (method II). Finally, in method III, we have estimated the RM dispersion using the magnetic energy spectrum under the assumption of statistical isotropy. As shown in Fig. 5, all three methods give very similar results, with method II giving ∼10–15 per cent larger $\bar{\sigma}_{\rm RM}$, and thus for all subsequent results of $\bar{\sigma}_{\rm RM}$, we mostly use method I.

On analysing the suite of fluctuation dynamo simulations, we show that the value of $\bar{\sigma}_{\rm RM}$ after the dynamo saturates is very similar for all the runs. In particular, $\bar{\sigma}_{\rm RM} = 0.4$–$0.5$ in the saturated state is independent of $P_{\rm M}$, $R_{\rm M}$ and the resolution of the run (see Figs 7 and 9, and the last two columns of Table 2). In addition, $\bar{\sigma}_{\rm RM}$ of this order is also obtained for an independent higher resolution (1024^3) and higher Reynolds number simulation of fluctuation dynamo from the JHU data base (last row of Table 2). This is a fairly large value for an intermittent random field, as it is of the order of 40–50 per cent of that expected in a model where $B_{\rm rms}$ strength fields volume fill each turbulent cell, but are randomly oriented from one cell to another.

We also find that the regions with a field strength larger than $2B_{\rm rms}$ contribute only 15–20 per cent to the total RM. Thus, the reduction in the RMs calculated after one cuts off the $2B_{\rm rms}$ fields is quite small. On the other hand, if one removes regions with a field strength larger than $1B_{\rm rms}$, then the RM decreases substantially, by a factor of 3 or so. These numbers obtain for both the 512^3 $P_{\rm M} = 1$ and $P_{\rm M} = 10$ runs.

The fact that cutting out the large-field regions does not significantly reduce the RM resulting from fluctuation dynamo generated

fields suggests the following picture. It shows that it is the general 'sea' of volume filling fluctuating fields that contribute dominantly to the RM produced by the fluctuation dynamo, rather than the high-field regions, right from the kinematic stage to the saturated state.

Moreover, in all cases, we find that $\bar{\sigma}_{\rm RM}$ and $L_{\rm int}$ begin to increase from their value in the kinematic stage, at the onset of saturation, when the influence of Lorentz forces becomes important. Therefore, the effect of Lorentz forces due to the fluctuation dynamo generated field is to order the field to larger and larger scale up to almost a universal maximum value. This maximum value seems to only depend on the forcing scale, and importantly is independent of the $P_{\rm M}$ and $R_{\rm M}$ to the extent we have tested. It would be important to do even higher $R_{\rm M}$ and $P_{\rm M}$ simulations in the future to firm up these conclusions.

Note that from equation (5), the dispersion in the normalized RM ($\bar{\sigma}_{\rm RM}$) is related to the integral scale of the magnetic field, $L_{\rm int}$, as defined in equation (6). Thus, the discussions above bring to fore also the evolution of the magnetic integral scale in the simulations of fluctuation dynamos. In the kinematic stage, $L_{\rm int}$ does depend on $R_{\rm M}$ and $P_{\rm M}$; we find that lower the $R_{\rm M} = Re$ or higher the $P_{\rm M}$, larger is the magnetic integral scale in the kinematic stage. This can be understood by studying the $R_{\rm M}(k)$ spectra and the eddy turnover rate spectra (see Fig. 10). We find that the first eddies which amplify the field efficiently are larger for runs with higher $P_{\rm M}$ or lower $R_{\rm M} = Re$, as they have a larger turnover rate and also their corresponding $R_{\rm M}(k)$ is supercritical. This then leads also to a correspondingly larger $L_{\rm int}$ for cases with lower $R_{\rm M} = Re$ or higher $P_{\rm M}$.

The situation when the dynamo saturates is quite different. Although the manner in which fluctuation dynamos saturate is not the main focus of our work, our results on the evolution of the magnetic integral scale, $L_{\rm int}$, point to some interesting features of saturation. First, in the 512^3, $P_{\rm M} = 1$ case (run F), $L_{\rm int}$ increases from about 0.3 in the kinematic stage to $\sim$0.9 in the saturated stage, or by a factor of about 3. Such an increase, if not of the same magnitude, can be seen in all the runs, and begins always when the Lorentz forces become important. In contrast, the integral scale of the velocity field does not change appreciably in any of the runs. On saturation, the magnetic integral scale $L_{\rm int}$ is only a factor of $2-3$ smaller than the velocity integral scale $L^V_{\rm int}$ (defined in an identical manner). Also, the integral scales of the saturated magnetic field are very similar, with $L_{\rm int} \sim 1$, for all our runs though they have different $R_{\rm M}$ and $P_{\rm M}$. These features suggest that the integral scale of the magnetic field in the saturated state does not depend on the microscopic resistivity or viscosity. It therefore appears that Lorentz forces can indeed order the magnetic field and increase its coherence scale to be a modest fraction ($\sim 1/2-1/3$) of the velocity coherence scale as the fluctuation dynamo saturates.

The dispersion of the normalized RM obtained here $\sim$0.4–0.5 implies a dimensional $\sigma_{\rm RM} \sim 180$ rad m^{-2}, for parameters appropriate for galaxy clusters. This is sufficiently large to account for the observed Faraday rotation seen in these systems. One also obtains a similar estimate for LOS through a disc galaxy. The fluctuation dynamo will generate the first fields in any turbulent system like a young galaxy. Our result that the generated field is fairly coherent and can lead to significant RM, even in the absence of a mean-field generation, will be of interest when one detects RM from higher and higher redshift galaxies. The present detection of excess RM from Mg II systems is marginally consistent with theoretical expectations.

Note that our work is complementary to those which simulate large-scale structure formation including the formation of massive galaxy clusters and the resulting magnetic field generation (Dolag 2006; Xu et al. 2009, 2012; Ryu et al. 2012). The cosmological simulations typically have a modest resolution of a turbulent eddy, as they have to also accommodate scales of the order of a cluster radius and larger. On the other hand, we have driven the turbulence at a scale comparable to the box scale, so as to resolve the small-scale structure of the magnetic field as well as possible within a turbulent cell. Both types of simulations will be useful to get a complete picture of the magnetic field generation in say galaxy clusters.

Astrophysical systems typically have much higher Reynolds numbers than any simulation would be able to achieve in the near future. However, some of the basic features of fluctuation dynamos are expected to be stable to the increase in Reynolds numbers. There are simulations of fluctuation dynamos with $P_{\rm M} = 1$, at higher resolutions (implying higher Reynolds numbers) than what we have presented here (Haugen et al. 2003; HBD; Perlman et al. 2007; Li et al. 2008; Jones et al. 2011), which show qualitatively very similar kinetic and magnetic spectra. In fact, we find that the $\bar{\sigma}_{\rm RM}$ from the JHU 1024^3 simulation (Table 2) match our results. It appears that for $P_{\rm M} = 1$, resolution of current simulations is sufficient to get converging results. Systems with large $P_{\rm M}$ and large Re are more difficult to simulate and would require improved computing resources. Nevertheless, to the extent we have explored the larger $P_{\rm M}$ case, the value of $\bar{\sigma}_{\rm RM}$ and hence the field coherence appear consistent with the $P_{\rm M} = 1$ case.

We have concentrated in the present paper on the RM signals from the fluctuation dynamo generated fields. It will also be of interest to study other observables, like the synchrotron emissivity and polarization signals. As the synchrotron emissivity depends non-linearly on the field strength, these signals would be more sensitive to the more intense and rarer structures, compared to the RM signal. It will also be of great interest to explore the results obtained here with higher resolution simulations, and also obtain an improved understanding of how fluctuation dynamos saturate, which remains a challenge.

ACKNOWLEDGMENTS

PB thanks Sharanya Sur for initial help with the PENCIL CODE. We thank Greg Eyink for alerting us to the JHU data base. We also thank Greg Eyink, Axel Brandenburg and R. Srianand for very useful discussions. We acknowledge the use of the HPC facility at IUCAA. KS acknowledges partial support from NSF Grant PHY-0903797 while at the University of Rochester. KS thanks Eric Blackman and Greg Eyink for warm hospitality at Rochester and Baltimore during his visit there. We thank an anonymous referee for comments which have led to improvements to our paper.

REFERENCES

Arshakian T. G., Beck R., Krause M., Sokoloff D., 2009, A&A, 494, 21
Balsara D. S., Kim J., 2005, ApJ, 634, 390
Beck R., 2012, Space Sci. Rev., 166, 215
Beck A. M., Lesch H., Dolag K., Kotarba H., Geng A., Stasyszyn F. A., 2012, MNRAS, 422, 2152
Beresnyak A., 2012, Phys. Rev. Lett., 108, 035002
Bernet M. L., Miniati F., Lilly S. J., Kronberg P. P., Dessauges-Zavadsky M., 2008, Nat, 454, 302
Binney J., Tremaine S., 1987, Galactic Dynamics. Princeton Univ. Press, Princeton
Bonafede A., Feretti L., Murgia M., Govoni F., Giovannini G., Dallacasa D., Dolag K., Taylor G. B., 2010, A&A, 513, A30
Bonafede A., Govoni F., Feretti L., Murgia M., Giovannini G., Brüggen M., 2011, A&A, 530, A24

Bouché N., Hohensee W., Vargas R., Kacprzak G. G., Martin C. L., Cooke J., Churchill C. W., 2012, MNRAS, 426, 801
Brandenburg A., 2003, Computational Aspects of Astrophysical MHD and Turbulence. Taylor and Francis Group, London, p. 269
Brandenburg A., Dobler W., 2002, Comput. Phys. Commun., 147, 471
Brandenburg A., Subramanian K., 2005, Phys. Rep., 417, 1
Brandenburg A., Sokoloff D., Subramanian K., 2012, Space Sci. Rev., 169, 123
Carilli C. L., Taylor G. B., 2002, ARA&A, 40, 319
Cho J., Ryu D., 2009, ApJ, 705, L90 (CR09)
Cho J., Vishniac E. T., 2000, ApJ, 538, 217
Cho J., Vishniac E. T., Beresnyak A., Lazarian A., Ryu D., 2009, ApJ, 693, 1449
Churazov E. et al., 2012, MNRAS, 421, 1123
Churchill C. W., Kacprzak G. G., Steidel C. C., 2005, in Williams P., Shu C.-G., Menard B., eds, IAU Colloq. 199: Probing Galaxies through Quasar Absorption Lines. Cambridge Univ. Press, Cambridge, p. 24
Clarke T. E., Kronberg P. P., Böhringer H., 2001, ApJ, 547, L111
de Avillez M. A., Breitschwerdt D., 2005, A&A, 436, 585
Dolag K., 2006, Astron. Nachr., 327, 575
Enßlin T. A., Vogt C., 2006, A&A, 453, 447
Eyink G. L., 2011, Phys. Rev. E, 83, 056405
Federrath C., Chabrier G., Schober J., Banerjee R., Klessen R. S., Schleicher D. R. G., 2011, Phys. Rev. Lett., 107, 114504
Felten J. E., 1996, in Trimble V., Reisenegger A., eds, ASP Conf. Ser. Vol. 88, Clusters, Lensing, and the Future of the Universe. Astron. Soc. Pac., San Francisco, p. 271
Fletcher A., 2011, arXiv:1104.2427
Gent F. A., Shukurov A., Fletcher A., Sarson G. R., Mantere M. J., 2012, arXiv:1204.3567
Govoni F., Feretti L., 2004, Int. J. Mod. Phys. D, 13, 1549
Govoni F. et al., 2010, A&A, 522, A105
Gradshteyn I. S., Ryzhik I. M., Jeffrey A., Zwillinger D., 2000, Table of Integrals, Series, and Products. Academic Press, Waltham
Gressel O., Elstner D., Ziegler U., Rüdiger G., 2008, A&A, 486, L35
Haugen N. E. L., Brandenburg A., Dobler W., 2003, ApJ, 597, L141
Haugen N. E., Brandenburg A., Dobler W., 2004a, Phys. Rev. E, 70, 016308 (HBD)
Haugen N. E. L., Brandenburg A., Mee A. J., 2004b, MNRAS, 353, 947
Iapichino L., Schmidt W., Niemeyer J. C., Merklein J., 2011, MNRAS, 414, 2297
Jones T. W., Porter D. H., Ryu D., Cho J., 2011, Mem. Soc. Astron. Ital., 82, 588
Kazantsev A. P., 1968, Sov. J. Exp. Theor. Phys., 26, 1031
Korpi M. J., Brandenburg A., Shukurov A., Tuominen I., Nordlund Å., 1999, ApJ, 514, L99
Kuchar P., Enßlin T. A., 2011, A&A, 529, A13
Kulsrud R. M., Anderson S. W., 1992, ApJ, 396, 606
Kulsrud R. M., Cen R., Ostriker J. P., Ryu D., 1997, ApJ, 480, 481
Li Y. et al., 2008, J. Turbulence, 9, 31
Monin A. S., Yaglom A. M., 1975, Statistical Fluid Mechanics: Mechanics of Turbulence. MIT Press, Cambridge, MA
Murgia M., Govoni F., Feretti L., Giovannini G., Dallacasa D., Fanti R., Taylor G. B., Dolag K., 2004, A&A, 424, 429
Nestor D. B., Johnson B. D., Wild V., Ménard B., Turnshek D. A., Rao S., Pettini M., 2011, MNRAS, 412, 1559
Norman M. L., Bryan G. L., 1999, in Röser H.-J., Meisenheimer K., eds, Lecture Notes in Physics, Vol. 530, The Radio Galaxy Messier. Springer-Verlag, Berlin, p. 106
Noterdaeme P., Srianand R., Mohan V., 2010, MNRAS, 403, 906
Paul S., Iapichino L., Miniati F., Bagchi J., Mannheim K., 2011, ApJ, 726, 17
Perlman E., Burns R., Li Y., Meneveau C., 2007, Supercomputing SC07, ACM, IEEE
Ryu D., Kang H., Cho J., Das S., 2008, Sci, 320, 909
Ryu D., Schleicher D. R. G., Treumann R. A., Tsagas C. G., Widrow L. M., 2012, Space Sci. Rev., 166, 1
Samui S., Subramanian K., Srianand R., 2010, MNRAS, 402, 2778
Sanders J. S., Fabian A. C., 2012, MNRAS, 421, 726
Sanders J. S., Fabian A. C., Smith R. K., Peterson J. R., 2010, MNRAS, 402, L11
Sanders J. S., Fabian A. C., Smith R. K., 2011, MNRAS, 410, 1797
Schekochihin A. A., Cowley S. C., Taylor S. F., Maron J. L., McWilliams J. C., 2004, ApJ, 612, 276
Schekochihin A. A., Cowley S. C., Kulsrud R. M., Hammett G. W., Sharma P., 2005, ApJ, 629, 139
Schleicher D. R. G., Banerjee R., Sur S., Arshakian T. G., Klessen R. S., Beck R., Spaans M., 2010, A&A, 522, A115
Schober J., Schleicher D., Federrath C., Glover S., Klessen R. S., Banerjee R., 2012, ApJ, 754, 99
Schuecker P., Finoguenov A., Miniati F., Böhringer H., Briel U. G., 2004, A&A, 426, 387
Shukurov A., 2004, Mathematical Aspects of Natural Dynamos. EDP Press, Norwich
Subramanian K., 1999, Phys. Rev. Lett., 83, 2957 (S99)
Subramanian K., Shukurov A., Haugen N. E. L., 2006, MNRAS, 366, 1437 (SSH)
Sur S., Federrath C., Schleicher D. R. G., Banerjee R., Klessen R. S., 2012, MNRAS, 423, 3148
Tobias S. M., Cattaneo F., Boldyrev S., 2011, arXiv:1103.3138
Vacca V., Murgia M., Govoni F., Feretti L., Giovannini G., Orra E., Bonafede A., 2010, A&A, 514, A71
Vazza F., Brunetti G., Gheller C., Brunino R., Brüggen M., 2011, A&A, 529, A17
Vogt C., Enßlin T. A., 2005, A&A, 434, 67
Wu Q., Kim J., Ryu D., Cho J., Alexander P., 2009, ApJ, 705, L86
Xu H., Li H., Collins D. C., Li S., Norman M. L., 2009, ApJ, 698, L14
Xu H. et al., 2012, ApJ, 759, 40
Zeldovich Y. B., Ruzmaikin A. A., Sokoloff D. D., 1990, The Almighty Chance. World Scientific Publishing Co. Pte. Ltd., Singapore

APPENDIX A: GENERAL ANALYTICAL DESCRIPTION OF RM DISPERSION

The Faraday RM for an LOS, 'L' from the source to the observer, parallel to z-axis and perpendicularly displaced by $\boldsymbol{r}_\perp$ from the centre of the cluster is given by

$$\mathrm{RM} = K \int_L n_\mathrm{e}(\boldsymbol{r}_\perp, z)\, B_z(\boldsymbol{r}_\perp, z)\mathrm{d}z. \tag{A1}$$

Here B_z is the component of the magnetic field in the z-direction. Then, the dispersion in RM along the LOS is given by

$$\langle(\mathrm{RM})^2\rangle = K^2 \int\int n_\mathrm{e}(\boldsymbol{r}_\perp, z)\, n_\mathrm{e}(\boldsymbol{r}_\perp, z') \overline{B_z(\boldsymbol{r}_\perp, z)\, B_z(\boldsymbol{r}_\perp, z')}\, \mathrm{d}z\, \mathrm{d}z',$$

where we have assumed that the density and magnetic field are not correlated. We define the relative coordinate $r_z = z' - z$ and the mean $Z = (z + z')/2$. For a random weakly inhomogeneous and isotropic magnetic field, we write the magnetic correlator as $\overline{B_i(\boldsymbol{x})\, B_j(\boldsymbol{y})} = M_{ij}(\boldsymbol{r}; \boldsymbol{R})$, where $\boldsymbol{r} = (\boldsymbol{x} - \boldsymbol{y})$ and $\boldsymbol{R} = (\boldsymbol{x} + \boldsymbol{y})/2$. This correlator is supposed to vary rapidly with $\boldsymbol{r}$ but slowly with $\boldsymbol{R}$. We will also assume that the correlation scale of the field is small compared to the variation scale of the density. Then the RM dispersion can be written as

$$\langle(\mathrm{RM})^2\rangle = K^2 \int_{-\infty}^{\infty} \mathrm{d}Z\, n_\mathrm{e}^2(\boldsymbol{r}_\perp, Z) \int_{-\infty}^{\infty} \mathrm{d}r_z\, M_{zz}(r_z; \boldsymbol{r}_\perp, Z), \tag{A2}$$

$\boldsymbol{R} \equiv (\boldsymbol{r}_\perp, Z)$. Note that $M_{zz}(|r_z|)$ is exactly the longitudinal correlation function $M_L(r)$ (cf. S99). We define the longitudinal integral scale in the standard fashion as

$$L_L = \frac{\int_0^\infty M_{zz}(|r_z|; \boldsymbol{r}_\perp, Z)\, \mathrm{d}r_z}{M_{zz}(0; \boldsymbol{r}_\perp, Z)}.$$

Moreover, as $M_L(0; \boldsymbol{r}_\perp, Z) = B^2_{\rm rms}(\boldsymbol{r}_\perp, Z)/3$, we get

$$\langle ({\rm RM})^2 \rangle = \frac{2K^2}{3} \int_{-\infty}^{\infty} L_L \, n_{\rm e}^2(\boldsymbol{r}_\perp, Z) B^2_{\rm rms}(\boldsymbol{r}_\perp, Z) \, {\rm d}Z, \tag{A3}$$

where the factor 2 arises because the integral over r_z in equation (A2), over the intervals $(0, \infty)$ and $(-\infty, 0)$, contributes equally to L_L.

For a density and rms magnetic field of uniform strength across the LOS with length L, equation (A3) reduces to

$$\left\langle ({\rm RM})^2 \right\rangle \Big)^{1/2} = \sigma_{\rm RM} = K n_{\rm e} B_{\rm rms} \frac{\sqrt{L_{\rm int} L}}{2}, \tag{A4}$$

where we have substituted $L_L = 3L_{\rm int}/8$. This equation is identical to equation 10 of CR09, which they derived from a Fourier space analysis, and it leads to the equation (5) that we have used in calculation of RM as per method III.

Consider now the more general case when the density and rms magnetic field varies with the cluster radius We use the standard β-model for the electron number density profile, $n_{\rm e} \propto (1 + r^2/r_{\rm c}^2)^{-3\beta/2}$ ($r_{\rm c}$ is the cluster core radius) and also assume $B_{\rm rms} \propto n_{\rm e}^\gamma$. Then the dispersion in RM becomes

$$\langle ({\rm RM})^2 \rangle = \frac{2L_L}{3} \, K^2 \, n_0^2 \, B_0^2 \int_{-\infty}^{\infty} \frac{{\rm d}Z}{\left(1 + \frac{r_\perp^2 + Z^2}{r_{\rm c}^2}\right)^{3\beta(\gamma+1)}}, \tag{A5}$$

where $r_\perp = |\boldsymbol{r}_\perp|$. Also n_0 and B_0 are the central density and rms magnetic field strength, respectively. The integral over Z can be evaluated exactly to give (equation 4 of 3.241 in Gradshteyn et al. 2000)

$$\sigma_{\rm RM}(r_\perp) = \sigma_{\rm RM}(0) \left(1 + \frac{r_\perp^2}{r_{\rm c}^2}\right)^{-\frac{(6\beta(\gamma+1)-1)}{4}}, \tag{A6}$$

where

$$\sigma_{\rm RM}(0) = \frac{\pi^{1/4}}{\sqrt{3}} \, K n_0 B_0 \sqrt{r_{\rm c} \, L_L} \sqrt{\frac{\Gamma(3\beta(\gamma+1) - 0.5)}{\Gamma(3\beta(\gamma+1))}}. \tag{A7}$$

The same expression with the longitudinal correlation scale L_L replaced by the cell size l is given by Felten (1996), for the case $\gamma = 0$.

This paper has been typeset from a TEX/LATEX file prepared by the author.